*Bulletin of the New Zealand Society for Earthquake Engineering, Vol. 57, No. 4, December 2024*

# THE SIGNIFICANCE OF POLARISATION IN NEAR-FAULT GROUND MOTIONS – A CASE STUDY OF FEBRUARY 2023 KAHRAMANMARAS M7.7 EARTHQUAKE

**Saed Moghimi[1] and Salar Manie[2]**

(Submitted *April 2024*; Reviewed *June 2024*; Accepted *September 2024*)

**ABSTRACT**

This article presents a comprehensive study on directivity effects and impulsive signals in near-fault ground motions, focusing on the case of the Kahramanmaraş earthquake in February 2023. The study investigates the impact of polarisation on pulse-type and non-pulse-type ground motions by computing spectral acceleration values for 180-degree rotated components. The results demonstrate that pulse-type ground motions exhibit higher spectral acceleration values and higher levels of polarisation, particularly in the period ranges close to the pulse period. The findings highlight the significance of directivity effects in seismic hazard analyses and emphasise the need for accurate assessment of directivity effects in seismic design procedures.

https://doi.org/10.5459/bnzsee.1689

## INTRODUCTION

On February 6, 2023, at 04:17 local time (01:17 GMT), an earthquake with a moment magnitude (Mw) of 7.7 occurred on the Eastern Anatolian Fault Zone (EAFZ) in Turkey. The earthquake had an epicenter located in Pazarcık-Kahramanmaraş (N37.288°, E37.043°), approximately 40 km northwest of Gaziantep and 33 km southeast of Kahramanmaraş, with a focal depth of 8.6 km. Subsequently, nine hours later, at 13:24 local time (10:24 GMT), a second earthquake with a moment magnitude of 7.6 hit the Ekinözü-Elbistan-Kahramanmaraş region. The epicenter of the second earthquake was in (N38.089°, E37.239°), approximately 98 km northwest of Adıyaman and 62 km northeast of Kahramanmaraş, with a focal depth of 7.0 km. The earthquake's moment tensor solution indicates that the movement on the NE-SW oriented faults was mostly left-lateral strike-slip. The strike orientation is 233°, and the dip angle is 74° [1-5]. The initial seismic data suggests that the earthquake began on the Narlı Segment, south of EAFZ, and then propagated northward to the main branch of the fault. The earthquake subsequently ruptured the Pazarcık-Erkenek fault segments towards the NE direction and the Amanos segment towards the SW direction. This earthquake is an example of a complex earthquake structure that involves multiple ruptures as a result of the interaction of two separate fault systems: the East Anatolian Fault Zone and the East Mediterranean Ridge. The rupture propagated in two directions, with one segment propagating to the north-northeast and the other to the south-southeast. The northern end of the rupture exhibited thrusting, while the southern end exhibited strike-slip faulting.

If a seismometer is positioned in the direction of the fault's forward rupture, the recorded velocity may show a large, long-period pulse, known as a "directivity effect" [6-8], which is of great interest to earthquake engineers due to its unique impact on structures. These types of ground motions can be seen mostly in the fault-normal component of ground motion (for strike slip cases) within a range of 25 up to 30km distance from the fault.

The directivity effect is a result of the interaction between the seismic waves and the irregularities in the rupture surface, such as the geometry and roughness of the fault surface, and the heterogeneity of the rocks in the vicinity of the fault. As the rupture propagates along the fault, the seismic waves radiate outward from the rupture front. The waves traveling at a velocity close to the rupture propagation velocity, in the direction of rupture propagation, result in seismic waves arriving in a more coherent and focused manner, leading to high amplitude and short duration pulses. This is known as the forward directivity effect. On the other hand, the backward directivity occurs when the rupture propagates away from a site. This results in seismic waves that are more dispersed and arrive over a longer period, leading to a different ground motion profile. The directivity effect can be significant for structures located within a certain distance from the fault, where the amplified waves can impose larger demands and consequently greater damage to the structures.

In addition to the directivity, the ground motion polarisation effect known as directionality can also be critical specially in near-fault pulse-type ground motions, as in some of the rotated orientations. These ground motions can apply a significant demand on the structure (sometimes up to three times greater than the geometric mean component in the case of the maximum rotated component) [9-11]. The maximum rotated component is the orientation in the ground motion which exhibits the strongest pulse signal which was first introduced by Shahi and Baker (2014) [12]. Previous algorithms for classifying pulse-like ground motions typically considered the motion in a single orientation. Shahi and Baker (2014) [12] introduced an improved algorithm capable of identifying pulses at any orientation within multicomponent ground motions. Their method uses continuous wavelet transforms of two orthogonal components to pinpoint the orientations most likely to contain a pulse. These wavelet transform results are then used to extract pulses from the identified orientations. The orientation with the strongest pulse signal is referred to as the maximum rotated component. The detailed process of the pulse-identifying algorithm of Shahi and Baker (2014) [12] is discussed in the upcoming sections.

For example, in strike-slip earthquakes, the fault-normal orientation (perpendicular to the fault trace) is the component in which the directivity effect is mostly pronounced. This means

[1] *Corresponding Author, Research Scientist, National Resource Canada, Toronto, Canada, saed.moghimi@gmail.com*
[2] *Assistant Professor, Civil Engineering Department, Sanandaj Branch, Islamic Azad University, Sanandaj, Iran.*

that the velocity waveform will show a long-period impulsive signal in this direction, which can be particularly damaging to structures while in the fault-parallel orientation (parallel to the fault trace) lower amplitudes with less destructive effects can be observed.

In order to understand the importance of the issue consider a fault that passes through a metropolitan area with thousands of high-rise buildings. The possibility that some of these high-rise buildings will be exposed to records containing pulses (caused by directivity or local soil effects) is quite significant. In addition, due to a large number of high-rise buildings in big cities, it can be assumed that some of these buildings will be exposed to the maximum rotated component of the earthquake record containing the pulse, so that the possibility is by no means far-fetched and cannot be ignored. However, the most common Ground Motion Prediction Equations (GMPEs) like NGA-West1 [13, 14] and NGA-West2 [15, 16] GMPEs utilize horizontal spectral ordinates having equal probability in all orientations [e.g., GMRotI50 or GMRotD50 horizontal component definitions as proposed in Boore et al. [17] and Boore [18] in seismic hazard calculations and earthquake load estimations.

Now the key question is that what if the maximum rotated component of a near-fault pulse-type ground motion hits the high-rise building which has been designed with common seismic design spectra and has been evaluated through nonlinear time history analysis with horizontal as-recorded pairs of ground motions? While the limited number of seismic design codes obligate to use the fault-normal and fault-parallel components in nonlinear time history analysis and performance evaluations (ASCE/SEI 7-10) the most common building codes do not have such requirements. On the other hand, it is shown that even the fault-normal and fault-parallel components do not lead to the most critical responses and do not provide maximum responses for all earthquake demand parameters simultaneously [19]. It should be noted that the 2009 edition of the NEHRP provisions [20] as well as the 2010 edition of the ASCE 7-10 standards [21] have started to use the maximum direction component in the definition of horizontal design spectrum since the collapse probability would be reduced for structures designed against maximum direction spectral demands (BSSC 2009) [20].

Numerous studies in existing literature tackle the issue of directionality in order to reconcile the definitions of horizontal components. Beyer and Bommer [22], for instance, offer a set of expressions that can be used to convert one definition of the horizontal component to another. Among these definitions, they suggest empirical expressions to convert GMRotI50 to the maximum of the horizontally rotated component (GMRotD100), without distinguishing between recordings obtained near the fault or far from it. Chang et al. [23] quantified velocity pulses, categorized their effects, corrected pulse-like motions, and determined orientations of the strongest pulses, highlighting limitations in PGV-based orientation predictions. Huang et al. [24] examine the relationships between geomean-based (GMRotI50) and maximum direction horizontal component definitions specifically for records obtained near the fault. Shahi and Baker [12] propose conversion expressions for horizontal components between GMRotD50 and GMRotD100, without making any distinctions regarding records associated with directivity or non-directivity.

**Directionality Effect in Ground Motions**

The significance of ground motion components in structural design has evolved significantly in recent earthquake engineering practices. Early seismic codes primarily utilized the geometric mean of acceleration spectra for design spectra. However, modern standards such as ASCE-7 (2022) [25] now emphasise the use of the maximum spectral acceleration component, driven by the substantial variations observed when ground motion is rotated. This phenomenon, known as polarisation or directionality in earthquake engineering, underscores the importance of considering spectral amplitude variations across different directions.

It is common to conflate directionality with directivity, although they represent distinct concepts. Directionality refers to the polarisation effect, where spectral amplitudes vary with direction, whereas directivity relates to the appearance of velocity waveform pulses due to rupture propagation towards the site.

This study investigates and compares the significance of polarisation and the maximum rotated component for pulse-type ground motions with respect to non-pulse-type counterparts. The rupture propagation pattern and the good spatial distribution of stations around the causative faults of the Kahramanmaraş earthquake have provided valuable information about the near-fault ground motions. Since the faults that caused the earthquake pass through the cities like Kahramanmaraş and Osmaniye several buildings in these cities are supposed to experience the directivity effect due to their location with respect to fault trance and rupture propagation pattern.

**Classification of Ground Motions and Analysis of Directivity Effects**

The first step in this study involved the classification of the selected ground motions into pulse-type and non-pulse-type categories. The classification of ground motions into pulse-like or non-pulse-like categories presents a challenging task due to the presence or absence of visible pulses in the velocity time history. An approach developed by Baker [26] and later refined by Shahi and Baker [12] was employed to identify pulse-like ground motions using the wavelet analysis method, based on the analysis of a single component of the time history recording. In 2014, Shahi and Baker [12] proposed an improved algorithm capable of classifying multi-component ground motions as pulse-like or non-pulse-like. This approach utilizes wavelet transform results from two orthogonal components of ground motions to detect potential pulses from all orientations and subsequently identifies the orientation with the strongest impulsive signal.

In this study, the acceleration time series associated with stations located within 100 km distance from the epicenter of the main earthquake (Mw 7.7) were downloaded from the AFAD [40]. This data was utilized to identify the stations that recorded ground motions exhibiting directivity effects. Initially, the Baker [26] algorithm was applied to identify the pulses in the FN and FP components. Subsequently, the Shahi and Baker [12] algorithm was used to confirm the maximum rotated components of the ground motions displaying directivity effects. The spatial distribution of the stations exhibiting directivity effects was then analysed to gain a better understanding of the rupture propagation pattern and finite fault mechanism. The spatial distribution of the stations displaying directivity effects aligns well with the rupture propagation pattern, as reported in METU/EERC [27]. The calculation of source-to-site geometrical parameters for each station and the subsequent discussion of the results were also conducted.

In the subsequent phase of the study, the spectral acceleration values were computed for the 180-degree rotated ground motion components to investigate and assess the impact of polarisation on pulse-type and non-pulse-type ground motions. The results indicate that the spectral acceleration values of pulse-type ground motions surpass those of non-pulse-type ground motions with similar source-to-site distance and local

site effects. Furthermore, the results reveal that pulse-type records exhibit higher polarisation levels compared to non-pulse records, particularly in the period ranges close to the pulse period. As anticipated, the pulses are more discernible in the fault normal components rather than the fault parallel components. The findings of the study provide valuable insights into the behaviour of complex earthquakes and underscore the significance of directionality in directivity-induced near-fault ground motions. The observed amplification in the direction of rupture propagation highlights the necessity for accurate assessment of directivity effects in seismic hazard analyses. This is consistent with previously conducted research such as the directivity models of NGA-WEST2 which illustrate ground motion amplification values up to 2.2 which confirms that this effect cannot be ignored in seismic hazard assessments [28].

**Understanding Impulsive Signals in Earthquake Ground Motions**

Various phenomena can cause impulsive signals in earthquake ground motions, with the most common phenomenon known as forward rupture directivity. The shear dislocation typically propagates at velocities close to the shear-wave velocity when a fault ruptures. Seismic waves emitted from different points along the rupture front can arrive almost simultaneously at near-source sites aligned with the propagation path, leading to the interference manifested as a double-sided velocity pulse.

Pulse-like ground motions can also result from other phenomena, including fling step and basin or site effects. Fling step refers to the static offset experienced by sites near the fault plane, which can be caused by either wave propagation generated from finite dislocation or the plastic response of near-surface materials. The ground displacement time series exhibits a one-sided pulse due to this static offset [29]. Interference effects arising from wave entrapment phenomena observed at the edges of alluvial basins and narrowband signal amplification caused by site effects [30, 31] can also generate monochromatic waveforms with characteristics similar to directivity-induced pulse-like ground motions. However, the occurrence of pulse-like ground motions is not guaranteed at all sites near the fault rupture, as it primarily depends on the site-to-source geometry and focal mechanism [32]. While pulse-like records used to be rare in older ground-motion databases due to the scarcity of near-source records, recent seismic events occurring amidst dense accelerometric networks have provided increasing numbers of such examples [33, 34].

Various methodologies have been proposed in the literature to classify the pulse of ground motion, such as Baker [26], Shahi and Baker [12], Tang and Zhang [35], Zhai et al. [36], and [37]. These methods utilize empirical criteria, spectral-shape-based criteria, and energy considerations to detect pulse-like features in seismic waveforms. However, since these methods rely solely on information obtained from the ground-motion record, it is not always possible to attribute the detected pulse-like features to specific source-related phenomena like forward rupture directivity. Therefore, a more cautious approach is recommended, which involves using an automated algorithm to parse the ground-motion records and then manually characterizing the records through visual inspection of spectral and waveform shapes as an additional classification criterion. The basis for this approach is the pulse indicator (PI) score, calculated using the continuous wavelet transform algorithm proposed by Baker [26] (Equation 1):

$$\boldsymbol{PI} = \frac{\mathbf{1}}{\mathbf{1}+e^{-\mathbf{23.3}+\mathbf{14.6}(\boldsymbol{PGV\ ratio})+\mathbf{20.5}(\boldsymbol{energy\ ratio})}} \quad (1)$$

The PGV ratio is obtained by dividing the peak ground velocity (PGV) of the residual record by the PGV of the original record. The residual waveform is obtained by subtracting the extracted pulse-type waveform from the original waveform, and represents the remaining ground motion components that are not captured by the pulse. Similarly, the energy ratio is computed by dividing the energy of the residual record by the energy of the original record. The energy of the signal can be determined by calculating the cumulative squared velocity or by summing the squared discrete wavelet coefficients. In cases where the far-field records exhibit straightforward motion, the resulting velocity time history may resemble a pulse subjected to filtering by the soil's inelastic properties. To eliminate these far-field pulse-like motions, Baker recommended imposing a PGV threshold greater than 30 cm/s on the records. To quantitatively classify a record as near-fault, the following criteria proposed by Baker [26] should be met:

- The pulse indicator of the record should be greater than 0.85.
- The pulse should arrive early in the velocity time history.

The cumulative squared velocity (CSV) of both the original and extracted pulses should be calculated, and at least 10% of the total CSV of the extracted pulse should occur before 20% of the total CSV of the original signal CSV.

The PGV of the record should be greater than 30 cm/s.

Ground motions with a PI value between 0.15 and 0.85 fall into an ambiguous range and require classification as either pulse-like or non-pulse-like through visual inspection and expert opinion. The PI value alone can sometimes be misleading in identifying pulse-like ground motions. For instance, in cases of multi-pulse ground motions, the wavelet analysis method may yield small PI values despite the presence of apparent impulsive signals in the ground motion. This discrepancy occurs because the PGV ratio and energy ratio values are close to 1 in multi-pulse signals, resulting from high PGV residual and Energy residual values. Consequently, Equation 1 produces lower PI values. This situation highlights the importance of visual inspection in the classification process.

**Application of Baker's Method on Kahramanmaras Earthquake Mw7.7 in February 2023**

On February 6, 2023, a significant earthquake struck the Pazarcık-Kahramanmaraş region, measuring 7.7 on the moment magnitude scale. The tremors were detected by a comprehensive network of 280 strong motion stations that are operated by the Disaster and Emergency Management Authority of Turkey (AFAD [40]). These stations were strategically positioned within a range of 436 km from the epicenter and were designed to capture ground motion data accurately. Of the 30 stations considered for investigation, 4 stations due to the presence of improper signals and 4 stations with Rrup greater than 50 km were excluded from the study. The remaining 22 records were subjected to rigorous analysis to identify the characteristics of the ground motion (Table 1). Of these, 11 records were classified as non-pulse, while 11 records demonstrated impulsive characteristics.

These ground motions were rotated to the fault-normal (FN) and fault-parallel (FP) orientations using the following planer transformation equations [38]:

$$\ddot{\boldsymbol{u}}_{\boldsymbol{FP}} = \ddot{\boldsymbol{u}}_{\mathbf{1}}\cos(\boldsymbol{\beta_1}) + \ddot{\boldsymbol{u}}_{\mathbf{2}}\cos(\boldsymbol{\beta_2})$$
$$\ddot{\boldsymbol{u}}_{\boldsymbol{FN}} = \ddot{\boldsymbol{u}}_{\mathbf{1}}\sin(\boldsymbol{\beta_1}) + \ddot{\boldsymbol{u}}_{\mathbf{2}}\sin(\boldsymbol{\beta_2}) \quad (2)$$

where $\beta_1 = \alpha_{strike} - \alpha_1$, $\beta_2 = \alpha_{strike} - \alpha_2$, $\alpha_{strike}$ is the strike of the fault as shown in Figure 1, $\alpha_1$ and $\alpha_2$ are the azimuths of the instrument axes (here equal to 0 and 90 degrees respectively since the seismometers are installed in NS-EW direction). Stations displaying directivity indications satisfy the source-to-

site geometric parameters conditions defined by Somerville et [39] (Table 1). According to Somerville et al. [39] X.cos(θ) should be greater than 0.5 and θ less than 45° on average in the forward-directivity region for Mw>6.5 and for T>0.6s in which X(=s/FL) is the length ratio for strike-slip faults and θ is the azimuth angle between the fault plane and ray path to site for strike-slip faults. Station 4615 is situated precisely alongside the Narli segment [40]. Due to the differing azimuth and rupture direction compared to the main fault strand, this segment demonstrates independent behaviour in terms of rupture propagation.

Figure 2 shows data from accelerometric stations that were positioned within 100 km of the epicenter and recorded both ordinary and pulse-like ground motions during the M 7.7 mainshock. The figure provides a clear visual representation of the spatial distribution of the two types of ground motions and highlights the importance of source-to-site geometric parameters in the emergence of directivity-induced impulsive signals.

Figure 2 clearly illustrates that stations exhibiting directivity effects are predominantly situated in the southwest region, aligning with the direction of rupture. The rupture originates from the epicenter, denoted by the yellow star on the corresponding segment in the figure, and subsequently propagates towards the southeast along the designated segments. This pattern further supports the finite fault rupture system proposed in the preliminary report of METU/EERC [27].

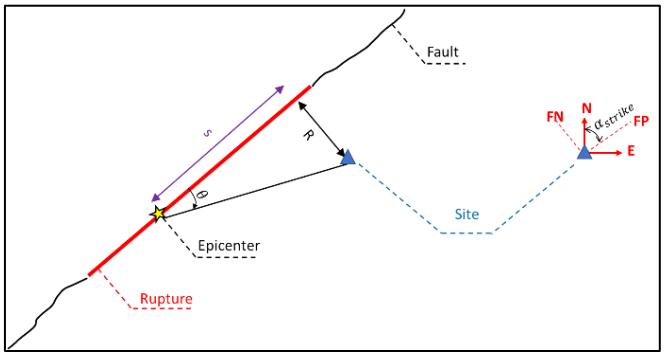


***Figure 1: Source to site geometric parameters for strike-slip faults (FN =Fault-normal; FP =Fault-parallel).***

***Table 1: List of downloaded records (stations).***

| Station | Latitude | Longitude | Vs30 (m/sec) | *Rrup* (km) | Theta(degree) | s (km) | FL (km) | X=s/FL | X.Cos(Theta) |
|---|---|---|---|---|---|---|---|---|---|
| **Pulse-like recorded motions** | | | | | | | | | |
| 3134 | 36.8276 | 36.2049 | 374 | 27.97 | 13 | 119.00 | 254.80 | 0.47 | 0.45 |
| 3137 | 36.6929 | 36.4885 | 688 | 2.29 | 1 | 118.29 | 254.80 | 0.46 | 0.46 |
| 3139 | 36.5838 | 36.4144 | 272 | 3.68 | 2 | 132.60 | 254.80 | 0.52 | 0.52 |
| 3143 | 36.8489 | 36.5571 | 444 | 0.00 | 0 | 101.05 | 254.80 | 0.40 | 0.40 |
| 3145 | 36.6454 | 36.4064 | 533 | 0.00 | 0 | 127.97 | 254.80 | 0.50 | 0.50 |
| 4615 | 37.3868 | 37.1380 | 484 | 0.00 | 0 | 13.84 | 32.42 | 0.43 | 0.43 |
| 4616 | 37.3755 | 36.8384 | 390 | 2.87 | 5 | 37.87 | 254.80 | 0.15 | 0.15 |
| 4624 | 37.5361 | 36.9177 | 280 | 11.85 | 10 | 69.05 | 254.80 | 0.27 | 0.27 |
| 4625 | 37.5387 | 36.9819 | 346 | 31.00 | 19 | 86.51 | 254.80 | 0.34 | 0.32 |
| 8002 | 37.1916 | 36.5620 | 430 | 11.62 | 26 | 23.55 | 254.80 | 0.09 | 0.08 |
| 8003 | 37.0842 | 36.2694 | 350 | 8.56 | 23 | 19.45 | 254.80 | 0.08 | 0.07 |
| **Non-pulse-like recorded motions** | | | | | | | | | |
| 2707 | 36.9309 | 36.5738 | 558 | 0.00 | 0 | 90.76 | 254.80 | 0.36 | 0.36 |
| 2709 | 37.1285 | 36.6705 | 555 | 0.00 | 0 | 67.11 | 254.80 | 0.26 | 0.26 |
| 3144 | 36.7569 | 36.4857 | 485 | 0.00 | 0 | 112.16 | 254.80 | 0.44 | 0.44 |
| 4611 | 37.7472 | 37.2843 | 731 | 18.87 | 132 | -16.80 | 254.80 | -0.07 | 0.04 |
| 4617 | 37.5855 | 36.8303 | 574 | 20.29 | 40 | 24.08 | 254.80 | 0.09 | 0.07 |
| 4618 | 37.6001 | 36.8723 | 715 | 16.88 | 39 | 20.78 | 254.80 | 0.08 | 0.06 |
| 4620 | 37.5857 | 36.8985 | 484 | 21.00 | 46 | 19.95 | 254.80 | 0.08 | 0.05 |
| 4621 | 37.5935 | 36.9291 | 714 | 16.07 | 42 | 17.71 | 254.80 | 0.07 | 0.05 |
| 4629 | 37.2874 | 36.7887 | 382 | 0.00 | 0 | 45.91 | 254.80 | 0.18 | 0.18 |
| 4630 | 37.3449 | 36.8060 | 347 | 4.08 | 6 | 41.66 | 254.80 | 0.16 | 0.16 |
| 4632 | 37.2560 | 36.7737 | 428 | 0.00 | 0 | 38.44 | 254.80 | 0.15 | 0.15 |

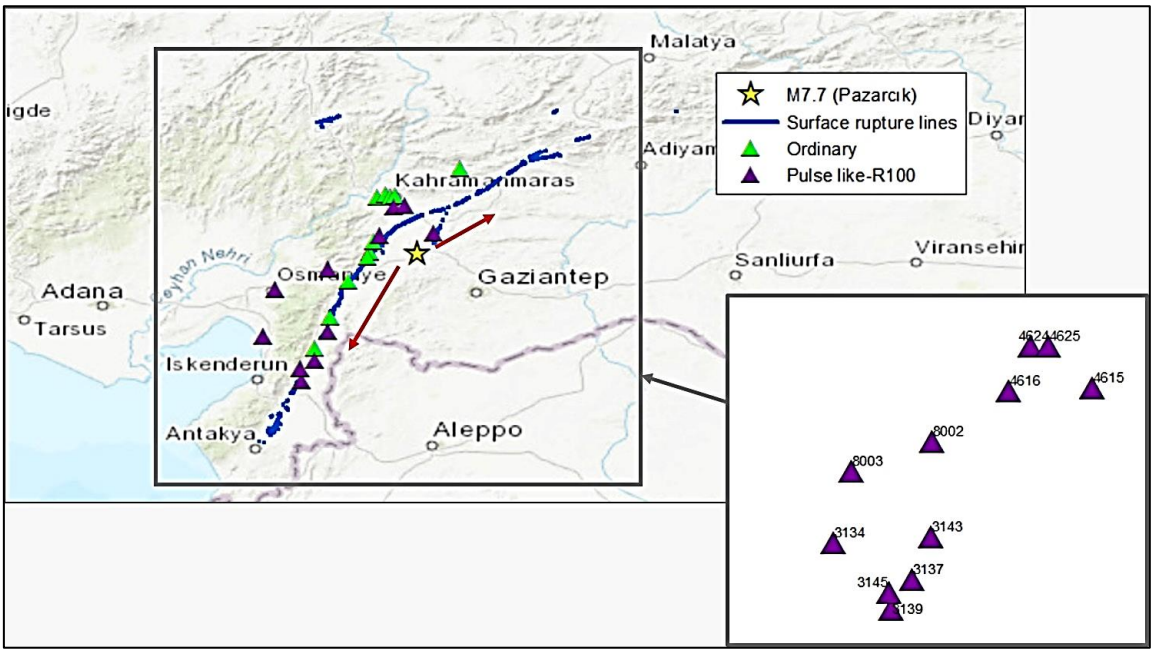


***Figure 2: Accelerometric stations that recorded both ordinary and pulse-like ground motions during the M 7.7. The star represents the earthquake epicenter.***

***Table 2: Results of pulse identification for stations.***

| Station ID | PGV Original | Maximum Rotated Ground Motion | | | | Fault Normal Direction | | |
|---|---|---|---|---|---|---|---|---|
| | | PI | Pulse Period | PGV Residual | Angle btw H1 and Strongest Orien. | PI | Pulse Period | PGV Residual |
| 3134 | 46.00 | 1.00 | 10.01 | 30.60 | 139 | 0.17 | 5.57 | 30.79 |
| 3137 | 84.89 | 1.00 | 9.14 | 51.30 | 123 | 0.04 | 13.76 | 63.27 |
| 3139 | 155.81 | 1.00 | 3.05 | 83.21 | 108 | 1.00 | 2.80 | 136.78 |
| 3143 | 149.69 | 1.00 | 7.15 | 100.39 | 137 | 0.01 | 15.62 | 59.41 |
| 3145 | 139.36 | 1.00 | 4.19 | 61.30 | 16 | 1.00 | 4.16 | 111.45 |
| 4615 | 130.72 | 1.00 | 5.17 | 46.91 | 112 | 0.92 | 3.84 | 78.60 |
| 4616 | 100.55 | 1.00 | 7.94 | 54.81 | 139 | 0.62 | 3.36 | 62.70 |
| 4624 | 67.08 | 0.30 | 4.98 | 54.17 | 76 | 0.45 | 4.98 | 73.65 |
| 4625 | 53.82 | 0.77 | 4.52 | 49.76 | 82 | 0.64 | 6.12 | 72.73 |
| 8002 | 40.18 | 1.00 | 8.81 | 27.46 | 150 | 0.00 | 1.43 | 27.10 |
| 8003 | 28.99 | 0.99 | 10.17 | 27.59 | 122 | 0.00 | 10.09 | 28.95 |

The methodology employed to analyse the ground motion data is described in detail below. The process consisted of utilizing the methods proposed by Baker [26] and Shahi and Baker [12], which facilitated the accurate identification of various types of observed ground motion during the earthquake. The specific steps undertaken are outlined as follows:

**Directivity Effect: Application of Baker's Methods [12,26]**

For each horizontal ground-motion record, we employed the continuous wavelet transform algorithm proposed by Baker [26]. The record was rotated across all non-trivial orientations, spanning 180°. Subsequently, the pulse indicator (PI) score was calculated. Table 2 presents the results, indicating that 11 records were identified as exhibiting an early-arriving pulse using Baker's method [26]. In this context, the pulse period refers to the pseudo-period of the most significant constituent wavelet present in the pulse-like ground motion. The PI score, ranging from 0 to 1, serves as a measure of the degree to which the local wavelet representation explains the velocity amplitude and energy content of the motion.

Higher PI scores indicate a greater likelihood of impulsive characteristics, while lower scores suggest ordinary ground motions without pulse-like features. According to the original algorithm, ground motions with PI scores equal to or greater than 0.85 are classified as pulse-like, while scores between 0.15 and 0.85 are considered ambiguous. Upon analysing the data, two sets of ground motions from Station 4624 and Station 4625 were identified as pulse-type waveforms through visual inspection. However, these two ground motions differ from other sets that are also verified as pulse-type. Specifically, at Station 4624, the waveform exhibits a very clear multi-pulse signal, whereas the directivity motions display a single dominant pulse. The pulse indicator parameter (Equation 1), used as a quantitative measure, can verify waveforms with a single clear pulse as pulse-type ground motion. This parameter employs the PGV Ratio and Energy Ratio to determine the

presence of a pulse. However, it can be misleading when earthquake signals contain multiple pulses. Even if the main pulse is extracted from the original signal, the PGV value of the residual signal remains high due to the presence of a second pulse. Consequently, the PGV Ratio will still be high, resulting in lower PI values, even though the existence of a pulse in the signal is evident. This scenario occurred at both Station 4624 and Station 4625. As demonstrated in Figure 3, the presence of a pulse is evident in the earthquake waveform of Station 4624, despite the lower PI values resulting from its multi-pulse nature. Therefore, these two ground motions from Station 4624 and Station 4625 are classified as pulse-type, non-directivity ground motions.

Figure 4 depicts the decomposition process employed on the ground motion component recorded at Station ID 8002 during the Mw 7.7 Kahramanmaras Earthquake. The figure showcases the original and residual ground velocity time histories following rotation at an azimuth of 150°. As a result of this rotation, a pulse period of 8.81 seconds is obtained. It is worth noting that the initial segment of the record contains the majority of the seismic energy, which serves as an indication of a pulse-like ground motion. This observation suggests that the ground motion at Station ID 8002 exhibits characteristics consistent with a pulse-like waveform.

Figure 5 displays the acceleration and velocity time series of the Fault Normal Component (FN) for the Mw 7.7 earthquake record at the same Station (8002). Despite the clear presence of an impulsive signal in the maximum rotated orientation, a distinct pulse signal is not visually identifiable in the fault-normal component, particularly at the beginning of the velocity waveform, which is expected in directivity ground motions. The wavelet analysis results also confirm this visual observation, showing a PI value of 0 in the fault normal case. Therefore, the fault normal component should be categorized as non-pulse-type ground motion. This example underscores the importance of considering polarisation (directionality) when evaluating near-fault pulse-type ground motions.

**Pulse Period**

The response of oscillators and structures is significantly influenced by the pulse period. When a pulse is present, systems with periods similar to the pulse period exhibit greater amplification in the response spectrum and structural response. Since wavelets lack a precise definition of period, the pulse period is determined by identifying the period associated with the highest Fourier amplitude of the wavelet, also known as the pseudo-period. In cases where multiple potential pulses exhibit pulse-like characteristics, the dominant pulse (with the highest wavelet coefficient) is selected, and its period is considered representative of the pulse period at a specific location. The amplification of spectral acceleration (Sa) resulting from the presence of a pulse-like feature in ground motion depends on the pulse period. Previous studies have shown a correlation between the pulse period and earthquake magnitude, which has been modelled using the modified classification algorithm [26, 39, 41, 42]. In order to investigate the relationship between pulse period and earthquake magnitude, Shahi and Baker [12] calculated the periods of all identified pulses. The period associated with the highest Fourier amplitude of the extracted pulse was considered as the measure of the pulse period, following the approach described by Shahi and Baker [12]. In cases where ground motions exhibited pulses in various orientations, the average period of all identified pulses was used as the representative pulse period ($T_p$) for the record. A linear regression analysis was conducted between the natural logarithm of $T_p$ and the earthquake magnitude, resulting in the following equation representing their relationship:

$$\mu_{lnT_P} = -5.73 + 0.99M \quad (3)$$

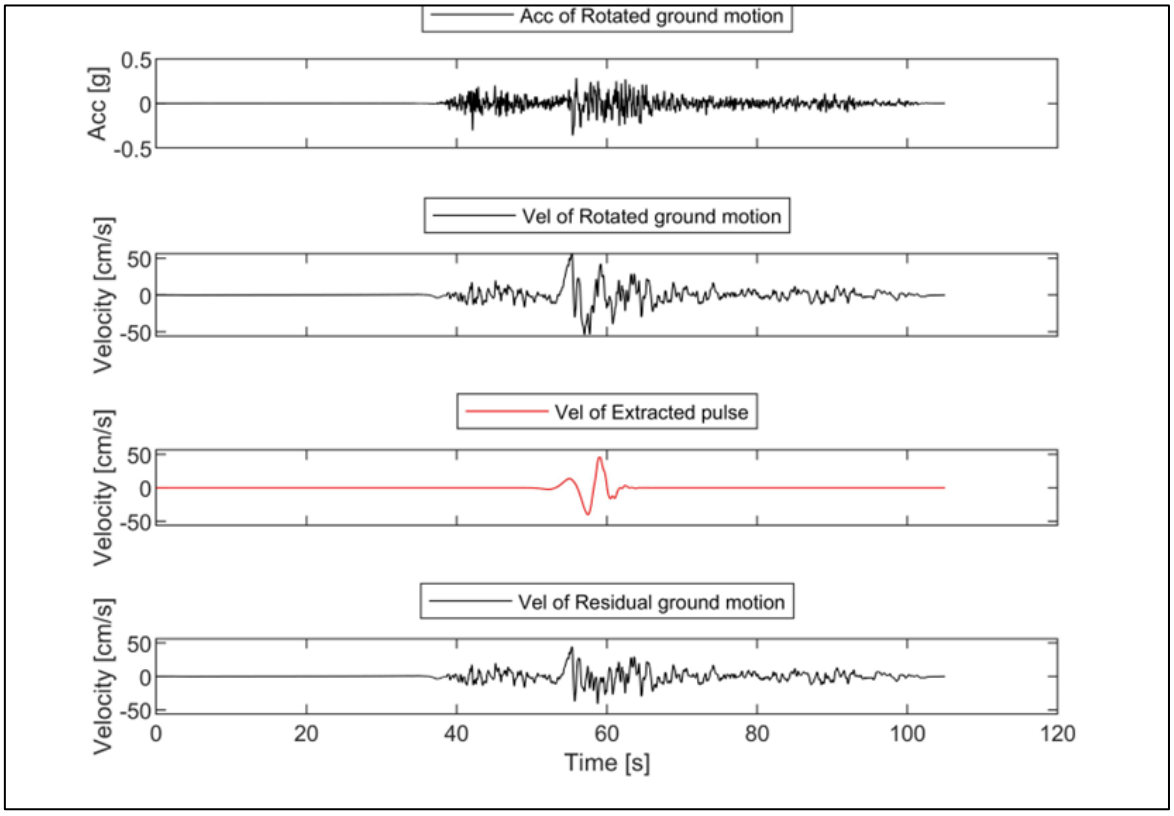


***Figure 3: Time series of ground acceleration and velocity for the Mw 7.7 earthquake record at Station 4624.***

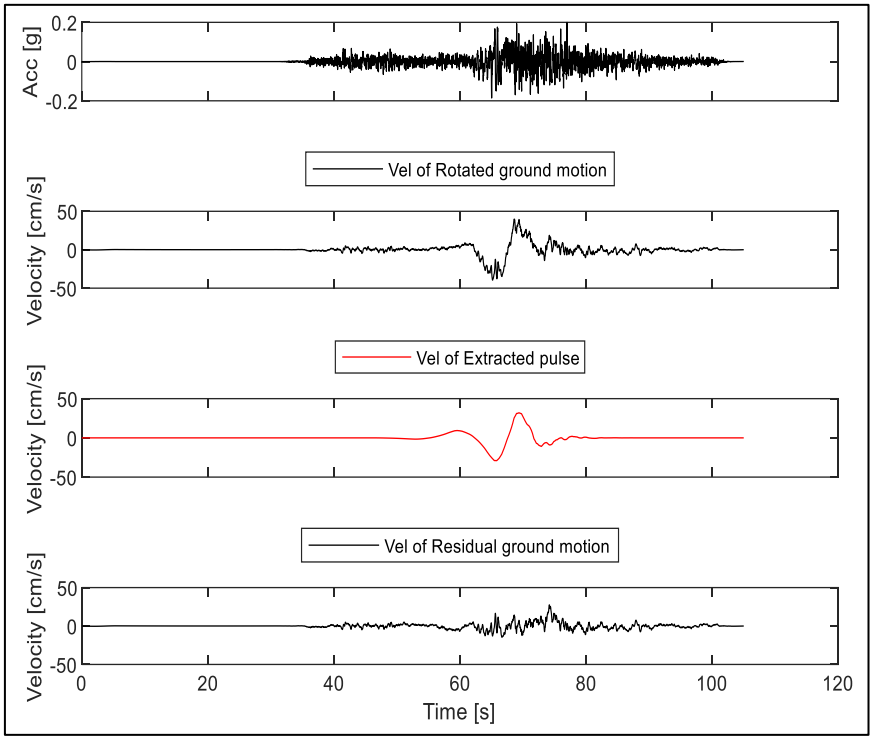


***Figure 4: Time series of ground velocity showing the maximum first PI (Pulse Indicator) value at the orientation with the highest score for the Mw 7.7 earthquake record at Station 8002.***

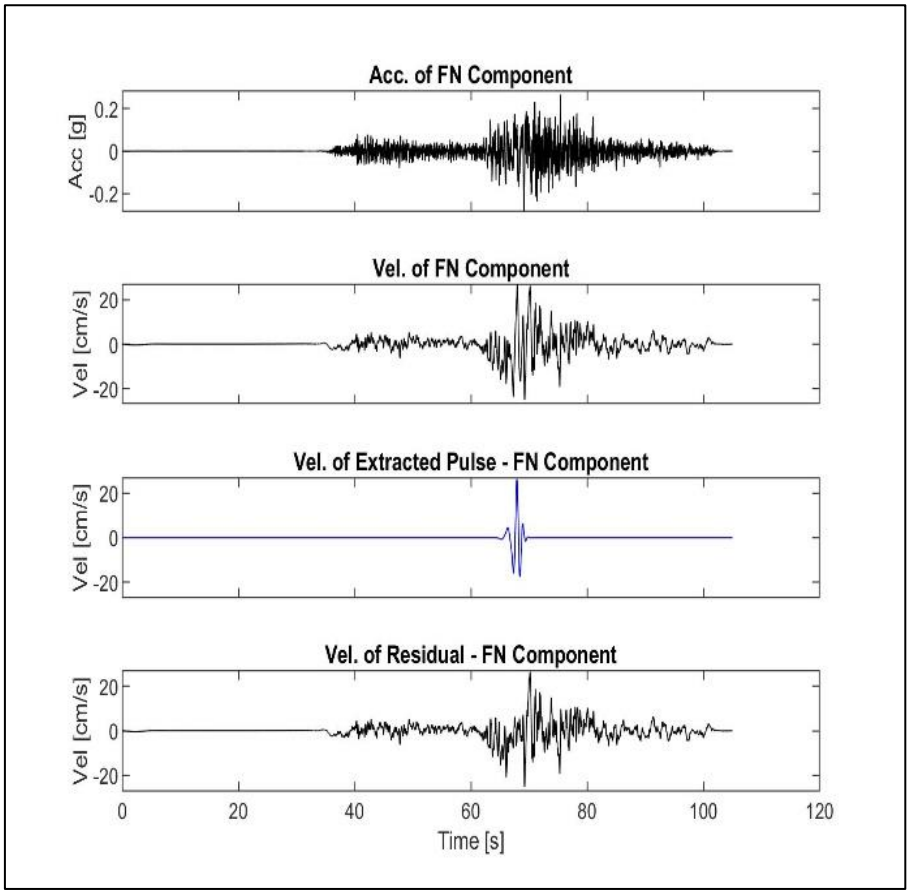


***Figure 5: Time series of ground acceleration and velocity showing the fault normal direction (FN) for the Mw 7.7 earthquake record at Station 8002.***

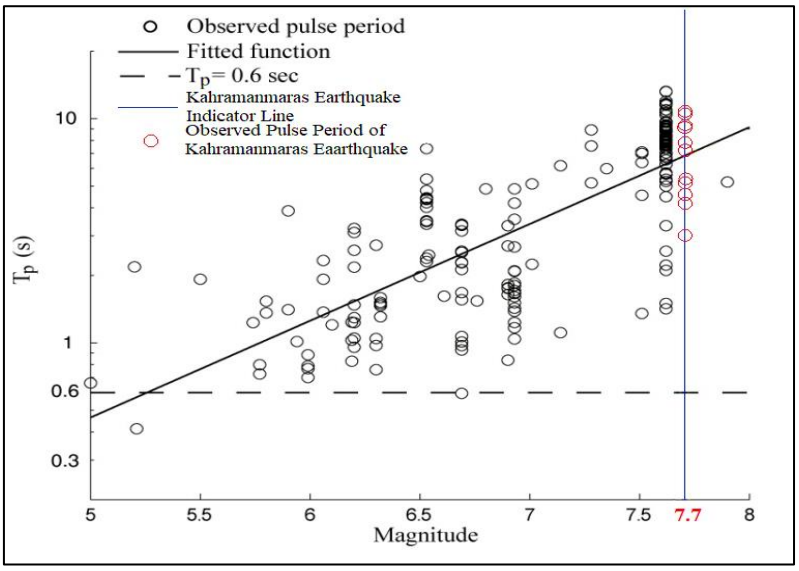


***Figure 6: Pulse period versus earthquake magnitude (Modified from [28] - Figure 2.8).***

Figure 6 (Modified from [43]) presents the average $T_p$ and magnitude (M) values, along with the equation-derived relationship, in addition to the observed pulse period of the Kahramanmaras Earthquake. The median $T_p$ (6.36 s) for the pulse period of the Kahramanmaras Earthquake aligns well with Equation 3, which predicts a median $T_p$ value of 6.63 s for a 7.7 magnitude earthquake.

**Local Site Effect**

The behaviour of soil significantly influences ground motion during earthquakes, making it crucial to consider its impact. Pulse-type ground motions are recorded at stations with softer soil types, where the Vs30 values range from 272 m/s to 688 m/s, with a mean value of 417 m/s. In contrast, non-pulse-type ground motions are observed at stations with a broader and stiffer range of soil types, where the Vs30 values range from 347 m/s to 731 m/s, with a mean value of 543 m/s.

If the pulse period of the ground motion is close to the natural period of the soil profile, the amplitude of the impulsive signal is expected to be amplified by local site effects. Soft soil basins amplify ground motions in higher period ranges. When the ground motion itself contains long-period impulsive signals due to directivity, this amplification becomes more crucial. Additionally, the effect of period elongation should not be ignored when the soil experiences strong ground motion and enters the nonlinear behaviour phase.

The natural period of soil is the period that the soil exhibits in the linear phase or during small deformations, referred to as the small-strain natural period. When the soil profile experiences strong excitation, its period can vary significantly from the small-strain natural period. As a result, a degraded-soil period, at least twice as long as the profile's small-strain natural period, can emerge. This degraded-soil period encompasses a broad range of periods with high response-spectral values. Therefore, the seismological effects of forward rupture directivity could be intensified due to soil amplification. Consequently, the amplification of seismic waves caused by the structure of the soil may further intensify the motion, making the effects of forward rupture directivity even more pronounced and resulting in a greater impact on the region.

It is worth noting that while this observation is significant, it is not the primary focus of our research, and a more detailed analysis is necessary to reach conclusive results.

**A Discussion on Directionality Effect**

In this earthquake, the selected records were divided into two categories: pulse and non-pulse. In this section, the importance of polarisation (directionality) will be examined for these two groups. Accordingly, the acceleration spectra were calculated for the resultant obtained by rotating the dual components of all records by 180 degrees. Thus, we have 180 acceleration spectra for each record. Among these 180 spectra, naturally, they encompass the response of all the components such as the as-recorded components (EW-NS), fault-normal (FN), fault-parallel (FP) components, geometric mean (GM), GMRotD50, and GMRotD100 in terms of spectral acceleration response. Additionally, the maximum rotated component [12] defined earlier was also computed for the pulse-type records. To compare these, we selected stations with compatible Rrup, Vs30, and source-to-site geometries. The slight differences in Vs30 and Rrup values can influence the overall amplitude of ground motions. However, the primary focus of this study was on the polarisation characteristics rather than absolute amplitudes. This comparison is meaningful because polarisation is primarily influenced by the directional characteristics of the ground motion waveform and is less sensitive to variations in amplitude due to soil type and rupture distance.

Figures 7a and 7b present pulse-type records at stations 3143 and 3139, with Vs30 values of 272 and 444 m/s, and pulse period values of 7.15 s and 3.05 s, and Rrup values equal to 3.68 and 0 km, respectively. Non-pulse-type records are selected from stations 2709 and 4629, with Vs30 values of 555 and 382 m/s, respectively. The Rrup is 0 km for both of these stations. For a detailed presentation of polarisation beneath the spectra, polar plots were drawn for non-pulse records at periods of 2.5s, 5.0s, 7.5s, and 10s (Figure 7). In the case of pulse-type records, polar plots were also drawn at the same periods, but the one closest to the pulse period value ($T_p$) was displayed at the $T_p$ value. For instance, for station 3143 (pulse-type), the $T_p$ value is 7.15s. The data obtained for the 7.15s value were presented in the polar plots instead of 7.5s, and this plot was highlighted in blue. As observed in Figure 7, the spectral values of pulse-type records are higher compared to non-pulse records, and polarisation is more pronounced in pulse-type records. The maximum rotated and fault-normal directions are also depicted. Particularly at the $T_p$ value, the fault-normal direction is closer to the maximum rotated direction.

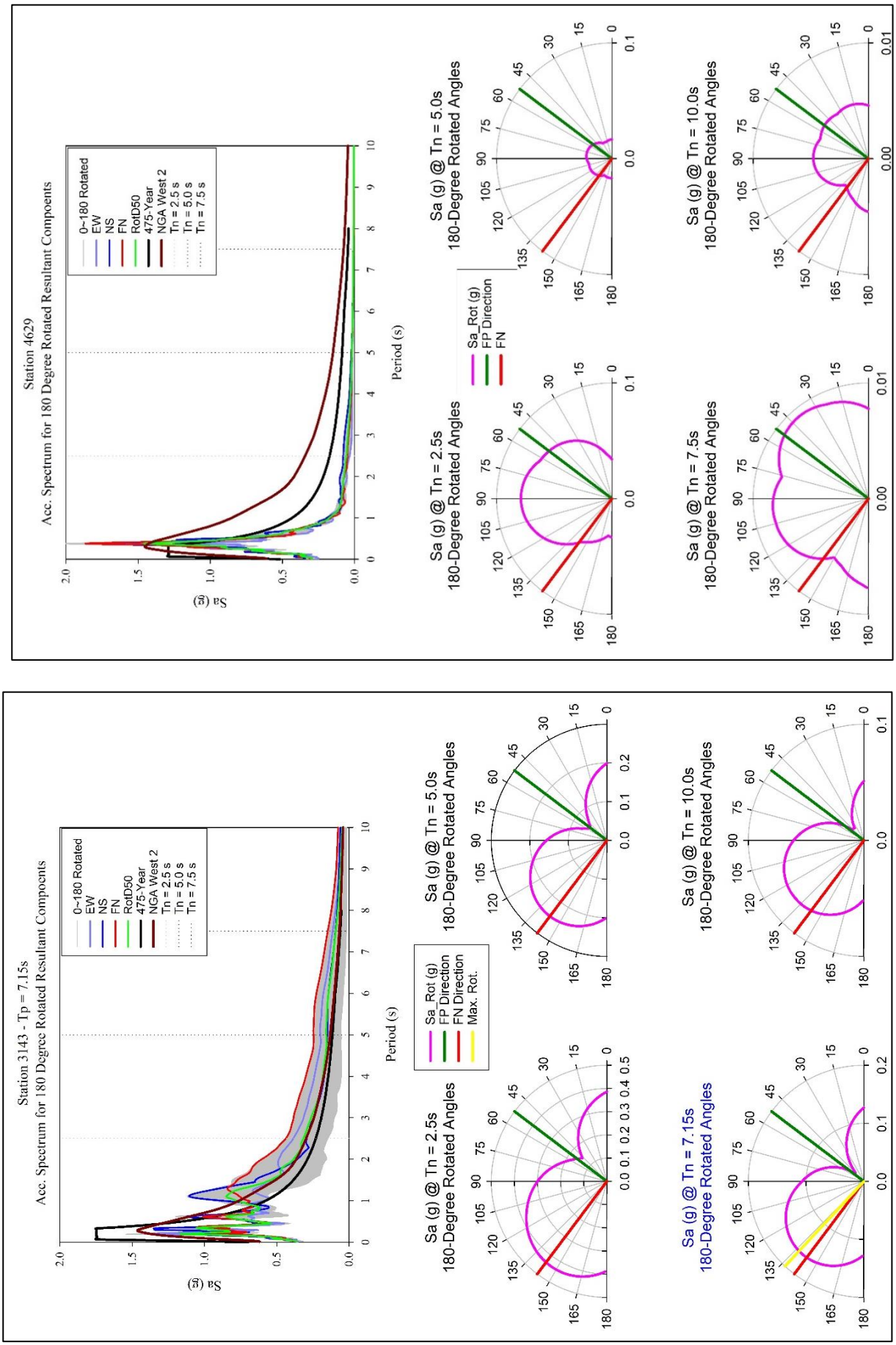


***Figure 7a: Comparison of spectrums and presentation of polarisation for a representative pulse type (3143) and non-pulse-type (4629) records.***

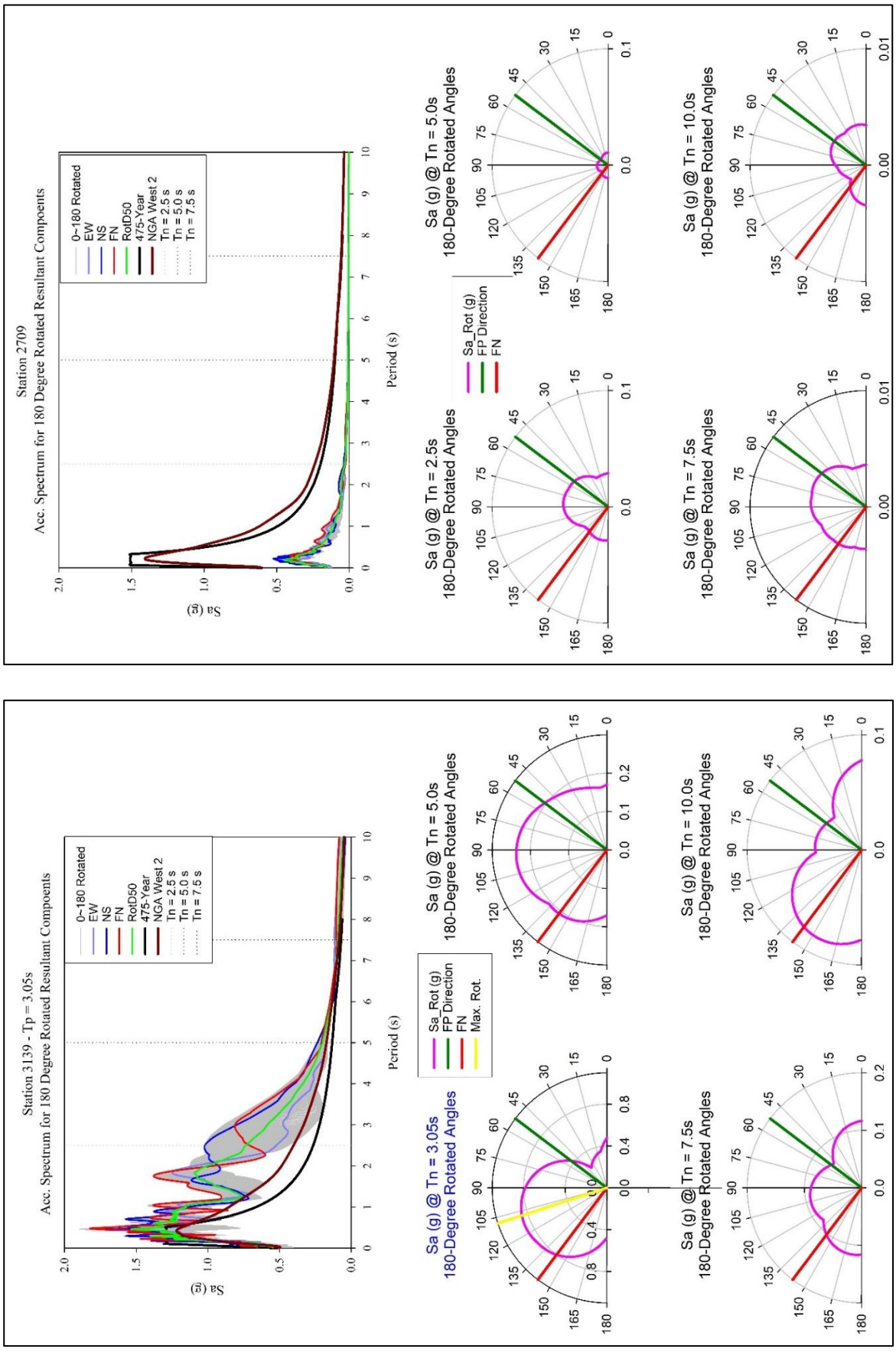


***Figure 7b: Comparison of spectrums and presentation of polarisation for a representative pulse type (3139) and non-pulse-type (2709) records.***

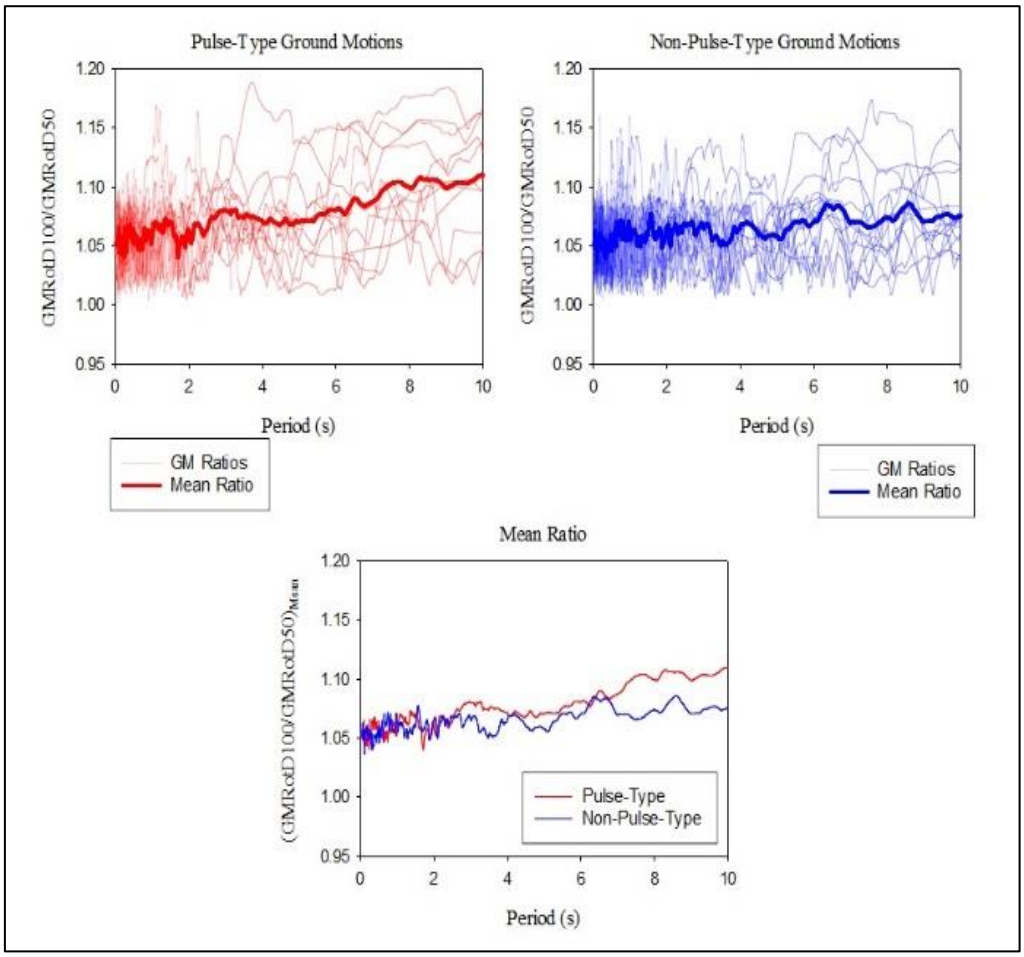


***Figure 8: GMRotD100/GMRotD50 ratios for pulse-type (a) and non-pulse-type (b) of records. Comparison of the median values of pulse-type and non-pulse-type records (c).***

The analysis of the 180-degree rotated spectra gives us a good idea of how polarized the records are. Although there is no a rigorous quantitative parameter for the polarisation measurement, GMRotD100/GMRotD50 ratio can give a generic insight about it. Here, we calculated the GMRotD100/GMRotD50 ratio for both types of records to demonstrate that polarisation is higher in pulse-type records. Figure 8a displays the ratio for the pulse-type ground motions and the corresponding median value of these ratios, while Figure 8b displays the ratios and the median value for non-pulse-type sets. As seen from these two figures, the GMRotD100 value can reach up to 20% higher than the GMRotD50 value for both pulse-type and non-pulse-type records. Figure 8c compares the median values of pulse-type and non-pulse-type records. When comparing the median values up to a period of 3 seconds, the ratios for pulse-type and non-pulse-type records are approximately the same. However, for periods larger than 3 seconds, pulse-type records show higher median ratios compared to non-pulse records.

This clearly indicates that pulse induces more polarisation because these intervals correspond to pulse periods. The results are consistent with previous findings for example Caltrans Seismic Design Criteria (SDC) [44], where the use of maximum direction (RotD100) horizontal spectral ordinates suggests an additional 15% to 25% spectral amplification compared to previously suggested amplifications to fully account.

The pronounced polarisation observed in pulse-type records, as evidenced by higher GMRotD100/GMRotD50 ratios, especially at longer periods, suggests that pulse-like ground motions may exhibit distinct directional properties that could impact structural response differently than non-pulse motions. This polarisation behaviour underscores the importance of considering waveform characteristics beyond spectral amplitudes in seismic hazard assessment and engineering design. Future research could further explore the implications of polarisation for structural resilience and inform mitigation strategies tailored to pulse-like ground motion scenarios.

## CONCLUSION

This article presents a comprehensive study on directivity effects and impulsive signals observed in near-fault ground motions, focusing on the case of the Kahramanmaraş earthquake in February 2023. The earthquake was a complex event involving multiple ruptures on the Eastern Anatolian Fault Zone and the East Mediterranean Ridge. The study aims to investigate the significance of polarisation in directivity-induced pulse-type ground motions and assess the behaviour of pulse-type ground motions compared to non-pulse-type motions. To classify the ground motions, a wavelet analysis-based approach developed by Baker (2007) and Shahi and Baker (2014) was utilized. The analysis revealed the presence of directivity effects in the fault-normal (FN) and fault-parallel (FP) components of the recorded ground motions. Spatial distribution analysis of stations exhibiting directivity effects provided insights into the rupture propagation pattern and finite fault mechanism. Furthermore, the study assessed the impact of polarisation on pulse-type and non-pulse-type ground motions by computing spectral acceleration values for rotated components. The results demonstrated that pulse-type motions exhibit higher polarisation levels and higher spectral acceleration values compared to non-pulse motions. Overall, this research sheds light on the behaviour of complex earthquakes, emphasizing the importance of considering

directivity effects in seismic hazard analyses and seismic design procedures. The findings highlight the necessity of accurate assessment and understanding of impulsive signals in near-fault ground motions to enhance the resilience of structures against earthquake-induced damage.

## REFERENCES


1 Barka AA and Kadinsky-Cade K (1988). "Strike-slip fault geometry in Turkey and its influence on earthquake activity". *Tectonics*, **7**(3): 663-684. https://doi.org/10.1029/TC007i003p00663

2 Ambraseys NN (1989). "Temporary seismic quiescence: SE Turkey". *Geophysical Journal International*, **96**(2): 311-331. https://doi.org/10.1111/j.1365-246X.1989.tb04453.x

3 McClusky S et al. (2000). "Global positioning system constraints on plate kinematics and dynamics in the eastern Mediterranean and Caucasus". *Journal of Geophysical Research: Solid Earth*, **105**(B3): 5695-5719. https://doi.org/10.1029/1999JB900351

4 Bulut F, Bohnhoff M, Eken T, Janssen C, Kılıç T and Dresen G (2012). "The East Anatolian Fault Zone: Seismotectonic setting and spatiotemporal characteristics of seismicity based on precise earthquake locations". *Journal of Geophysical Research: Solid Earth*. https://doi.org/10.1029/2011JB008966

5 Duman TY, Emre Ö (2013). "The East Anatolian Fault: geometry, segmentation and jog characteristics". *Geological Society London Special Publications*, **372**: 495-529. https://doi.org/10.1144/SP372.14

6 Somerville PG, Smith NF, Graves RW and Abrahamson NA (1997). "Modification of empirical strong ground motion attenuation relations to include the amplitude and duration effects of rupture directivity". *Seismological Research Letters*, **68**(1): 199-222. https://doi.org/10.1785/gssrl.68.1.199

7 Abrahamson NA (2000). "Effects of rupture directivity on probabilistic seismic hazard analysis". In *Proceedings of the 6th International Conference on Seismic Zonation*, Palm Springs, CA, **1**: 151-156.

8 Mavroeidis GP and Papageorgiou AS (2003). "A mathematical representation of near-fault ground motions". *Bulletin of the Seismological Society of America*, **93**(3): 1099-1131. https://doi.org/10.1785/0120020100

9 Watson-Lamprey J and Boore DM (2007). "Beyond SaGMRotI: Conversion to SaArb, SaSN, and SaMaxRot". *Bulletin of the Seismological Society of America*, **97**(5): 1511-1524. https://doi.org/10.1785/0120070007

10 Huang Y, Whittaker A and Luco N (2008). "Maximum spectral demands in the near-fault region". *Earthquake Spectra*, **24**(1): 319-341.

11 Huang YN, Whittaker AS and Luco N (2010). "NEHRP site amplification factors and the NGA relationships". *Earthquake Spectra*, **26**(2): 583-593. https://doi.org/10.1193/1.2830435

12 Shahi SK and Baker JW (2014). "An efficient algorithm to identify strong-velocity pulses in multicomponent ground motions". *Bulletin of the Seismological Society of America*, **104**(5): 2456-2466. https://doi.org/10.1785/0120130191

13 Campbell KW and Bozorgnia Y (2008). "NGA ground motion model for the geometric mean horizontal component of PGA, PGV, PGD and 5% damped linear elastic response spectra for periods ranging from 0.01 to 10s". *Earthquake Spectra*, **24**(1): 139-171. https://doi.org/10.1193/1.2857546

14 Power M, Chiou B, Abrahamson N, Bozorgnia Y, Shantz T and Roblee C (2008). "An overview of the NGA project". *Earthquake Spectra*, **24**(1): 3-21. https://doi.org/10.1193/1.2894833

15 Bozorgnia Y et al. (2014). "NGA-West2 research project". *Earthquake Spectra*, **30**(3): 973-987. https://doi.org/10.1193/072113EQS209M

16 Idriss IM (2013). "*NGA-West2 Model for Estimating Average Horizontal Values of Pseudo-Absolute Spectral Accelerations Generated by Crustal Earthquakes*". PEER Report 2013-08". Pacific Earthquake Engineering Research Center, University of California, Berkeley, CA.

17 Boore DM, Watson-Lamprey J and Abrahamson NA (2006). "Orientation-independent measures of ground motion". *Bulletin of the Seismological Society of America*, **96**(4A): 1502-1511. https://doi.org/10.1785/0120050209

18 Boore DM (2010). "Orientation-independent, nongeometric-mean measures of seismic intensity from two horizontal components of motion". *Bulletin of the Seismological Society of America*, **100**(4): 1830-1835. https://doi.org/10.1785/0120090400

19 Kalkan E and Kwong NS (2014). "Pros and cons of rotating ground motion records to fault-normal/parallel directions for response history analysis of buildings". *Journal of Structural Engineering*, **140**(3): 04013062. https://doi.org/10.1061/(ASCE)ST.1943-541X.0000845

20 BSSC (2009). "*NEHRP Recommended Seismic Provisions for New Buildings and Other Structures*". Federal Emergency Management Agency, Washington, DC.

21 ASCE7-10. (2010). "*SEI 7-10: Minimum Design Loads for Buildings and Other Structures*". American Society of Civil Engineers, USA.

22 Beyer K and Bommer JJ (2006). "Relationships between median values and between aleatory variabilities for different definitions of the horizontal component of motion". *Bulletin of the Seismological Society of America*, **96**(4A): 1512-1522. https://doi.org/10.1785/0120050210

23 Chang Z, Wu H, Li W, Yan Z, Peng L and Zhu G (2024). "Analysis of near-fault ground motions in the February 2023 Kahramanmaras, Türkiye, earthquake sequence". *Research Square Preprint (Version 1)*. https://doi.org/10.21203/rs.3.rs-4282319/v1

24 Huang Y, Wu J, Zhang T and Zhang D (2008). "Relocation of the M 8.0 Wenchuan earthquake and its aftershock sequence". *Science in China Series D: Earth Sciences*, **51**: 1703-1711. https://doi.org/10.1007/s11430-008-0135-z

25 ASCE (2022). "*Minimum Design Loads and Associated Criteria for Buildings and Other Structures*". American Society of Civil Engineers, USA.

26 Baker JW (2007). "Quantitative classification of near-fault ground motions using wavelet analysis". *Bulletin of the Seismological Society of America*, **97**(5): 1486-1501. https://doi.org/10.1785/0120060255

27 METU/EERC (2023). "*Kahramanmaras-Pazarcik and Elbistan Earthquakes Preliminary Report*". Report No. METU/EERC 2023-01.

28 Spudich P, Bayless JR, Baker JW, Chiou BS, Rowshandel B, Shahi SK and Somerville P (2013). "*Final Report of the NGA-West2 Directivity Working Group*". PEER Report 2103-09, Pacific Earthquake Engineering Research Center, University of California, Berkeley, CA.

29 Bolt B (2010). "*Engineering Seismology*" in Bozorgnia Y and Bertero VV (Editors), *Earthquake Engineering: from Engineering Seismology to Performance-Based Engineering*. CRC Press, New York.

30 Bradley BA and Cubrinovski M (2011). "Near-source strong ground motions observed in the 22 February 2011 Christchurch earthquake". *Bulletin of the New Zealand Society for Earthquake Engineering*, **44**(4): 181-194. https://doi.org/10.5459/bnzsee.44.4.181-194

31 Luzi L, D'Amico M, Massa M and Puglia R (2019). "Site effects observed in the Norcia intermountain basin (Central Italy) exploiting a 20-year monitoring". *Bulletin of Earthquake Engineering*, **17**: 97-118. https://doi.org/10.1007/s10518-018-0444-3

32 Iervolino I and Cornell CA (2008). "Probability of occurrence of velocity pulses in near-source ground motions". *Bulletin of the Seismological Society of America*, **98**(5): 2262-2277. https://doi.org/10.1785/0120080033

33 Chioccarelli E and Iervolino I (2010). "Near-source seismic demand and pulse-like records: A discussion for L'Aquila earthquake". *Earthquake Engineering and Structural Dynamics*, **39**(9): 1039-1062. https://doi.org/10.1002/eqe.987

34 Luzi L et al. (2017). "The central Italy seismic sequence between August and December 2016: Analysis of strong-motion observations". *Seismological Research Letters*, **88**(5): 1219-1231. https://doi.org/10.1785/0220170037

35 Tang Y and Zhang (2011). "Response spectrum-oriented pulse identification and magnitude scaling of forward directivity pulses in near-fault ground motions". *Soil Dynamics and Earthquake Engineering*, **31**(1): 59-76. https://doi.org/10.1016/j.soildyn.2010.08.006

36 Zhai C, Chang Z, Li S, Chen Z and Xie L (2013). "Quantitative identification of near-fault pulse-like ground motions based on energy". *Bulletin of the Seismological Society of America*, **103**(5): 2591-2603. https://doi.org/10.1785/0120120320

37 Chang Z, Wu H and Goda K (2024). "Automated parameterization of velocity pulses in near-fault ground motions". *Earthquake Engineering and Structural Dynamics*, **53**(3): 997-1005. https://doi.org/10.1002/eqe.4053

38 Reyes J and Kalkan E (2012). "Relevance of fault-normal/parallel and maximum direction rotated ground motions on nonlinear behaviour of multi-story buildings". *Proceedings of the 15th World Conference on Earthquake Engineering*, Lisbon, Portugal.

39 Somerville PG (2003). "Magnitude scaling of the near fault rupture directivity pulse". *Physics of the Earth and Planetary Interiors*, **137**(1-4): 201-212. https://doi.org/10.1016/S0031-9201(03)00015-3

40 AFAD (2023). "*06 Şubat 2023 Pazarcık-Elbistan Kahramanmaraş (Mw: 7.7- Mw: 7.6) Depremleri Raporu*". Deprem Dairesi Başkanlığı (in Turkish). https://deprem.afad.gov.tr/assets/pdf/Kahramanmaras%20%20Depremleri_%20On%20Degerlendirme%20Raporu.pdf

41 Alavi B and Krawinkler H (2004). "Behaviour of moment-resisting frame structures subjected to near-fault ground motions". *Earthquake Engineering and Structural Dynamics*, **33**(6): 687-706. https://doi.org/10.1002/eqe.369

42 Fu Q and Menun C (2004). "Seismic-environment-based simulation of near-fault ground motions". *Proceedings of the 13th World Conference on Earthquake Engineering*, Vancouver, Canada.

43 Shahi SK (2013). "*A probabilistic framework to include the effects of near-fault directivity in seismic hazard assessment*". Stanford University, CA, USA.

44 Caltrans (2013). "*Seismic Design Criteria. California Department of Transportation: Sacramento*". Version 1.7, CA, USA.